Probing interactions between core-electron transitions by ultrafast two-dimensional x-ray coherent correlation spectroscopy

Igor V. Schweigert and Shaul Mukamel[a)]
Department of Chemistry, University of California, Irvine, California 92697-2025, USA

(Received 27 August 2007; accepted 14 January 2008; published online 12 May 2008)

Two-dimensional x-ray correlation spectra (2DXCS) obtained by varying two delay periods in a time-resolved coherent all-x-ray four-wave-mixing measurement are simulated for the N 1*s* and O 1*s* transitions of aminophenol. The necessary valence and core-excited states are calculated using singly and doubly substituted Kohn–Sham determinants within the equivalent-core approximation. Sum-over-states calculations of the 2DXCS signals of aminophenol isomers illustrate how novel information about electronic states can be extracted from the 2D spectra. Specific signatures of valence and core-excited states are identified in the diagonal and off-diagonal peaks arising from core transitions of the same and different types, respectively. © *2008 American Institute of Physics*. [DOI: 10.1063/1.2839859]

I. INTRODUCTION

Near-edge x-ray absorption spectroscopy (XANES) is a powerful frequency-domain tool for studying the electronic structure of molecules.[1] The fine structure of the absorption spectrum reflects the electronic states in the vicinity of the absorbing atom and thus provides a probe for the molecular electronic environment with an atomic-scale resolution. X-ray pulses from high-harmonic generation (HHG) have made it possible to record changes in the XANES signal on an attosecond (as) scale, providing time-resolved information about the variations in the atomic positions or charge distribution triggered by an optical or ultraviolet pulse.[2–9] Much brighter femtosecond x-ray pulses will soon become available from the x-ray free electron lasers (XFEL). Further improvements of the HHG brilliance[9] as well as XFEL pulse quality and duration[10] should ultimately make it possible to perform time-domain coherent nonlinear experiments with multiple x-ray pulses. Current and proposed applications of the HHG and XFEL such as optical pump/x-ray probe or time-resolved absorption make use of the ultrafast nature of the pulses but do not exploit their coherent properties. Coherent all-x-ray techniques can probe multiple types of core transitions within the same experiment, improving the resolution and enhancing desired features via the use of elaborate pulse sequences, as is commonly done in nuclear-magnetic resonance.[11] They should provide more detailed information on the electronic structure and dynamics than available from XANES or its time-resolved variations.

We have recently formulated the principles of two-dimensional x-ray correlation spectroscopy[12] (2DXCS), an all-x-ray technique based on a coherent resonant four-wave-mixing measurement.[13,14] Two-dimensional correlation techniques originally introduced in nuclear-magnetic resonance[15] are now widely used in the infrared and visible regimes.[16] In general, the correlation spectrum is obtained by subjecting the system to a sequence of pulses and recording the coherent nonlinear response as a function of the various delay periods between consecutive pulses. The Fourier transform of the signal with respect to two such delays can be displayed as a 2D frequency correlation plot. By spreading the signal over multiple frequency axes, the weak signatures of interactions between different transitions can be separated from strong same-transition signals.[17] Transitions of the same type contribute to the diagonal part of the correlation spectrum, while features arising from interactions among spectrally-separated transitions appear in the off-diagonal "cross peaks." In addition, certain types of static inhomogeneous broadening can be eliminated by specific pulse sequences (e.g., the photon echo technique).

In this paper, the diagonal and off-diagonal components of the N 1*s* and O 1*s* 2DXCS signals of the three isomers of aminophenol are simulated and analyzed using the response function formalism[18] and the sum-over-states approach. The diagonal 2DXCS signal arising due to transitions from a single core shell consists of two Raman-type contributions that involve multiple valence and core excited states spanned by the pulse finite bandwidths. Transitions from valence-excited to core-excited states contribute to the negative-frequency part of the diagonal spectrum and can be clearly distinguished from the ground to core-excited transitions already visible in XANES. The 2DXCS cross peaks arising from the transitions involving two different core shells consist of two contributions, one involving transitions to singly core excited states and the other involving also transitions to states with two core electrons excited. The two contributions have opposite signs and cancel exactly if two core transitions are decoupled. Unlike XANES, which probes each core shell independently, the 2DXCS cross peaks probe the interactions between the transitions and thus are highly sensitive to the electronic environment in the vicinity of the two core shells.

Closed-form expressions for the 2DXCS signals in terms of the molecular eigenstates are derived in Sec. II. The dependence of the 2DXCS signals on three different (no core

a)Electronic mail: smukamel@uci.edu.

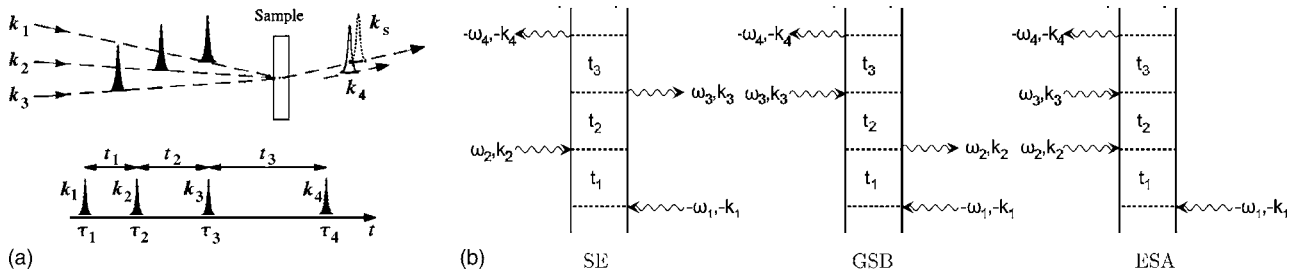

FIG. 1. (a) Pulse sequence in a four-wave mixing experiment. Three pulses $\boldsymbol{k}_1$, $\boldsymbol{k}_2$, and $\boldsymbol{k}_3$ induce a polarization in the molecule, which is probed by the heterodyne field $\boldsymbol{k}_4$. t_3,t_2,t_1 denote time intervals between consecutive pulses. (b) Double-sided Feynman diagrams representing the stimulated emission, ground-state bleaching, and excited-state absorption contributions to the polarization in the $\boldsymbol{k}_I=-\boldsymbol{k}_1+\boldsymbol{k}_2+\boldsymbol{k}_3$ direction [Eq. (8)].

hole, one core hole, and two core holes) excited-state manifolds makes it particularly challenging for a first-principles simulation. We use the equivalent-core approximation[19,20] (ECA), whereby the core transitions are described by the valence transitions of the equivalent-core molecule, which has modified nuclear configuration and an additional electron. Slater determinants made of occupied and unoccupied Kohn–Sham (KS) orbitals within the ECA are used to represent the valence and the core excited states as described in Sec. III. Doubly substituted determinants necessary to describe doubly core excited states are included. All three excited-state manifolds (valence, singly, and doubly core excited states) can thus be calculated with standard quantum chemistry codes.

The simulations are presented in Sec. IV. We show that while most peaks in the diagonal N/N signal arise from the same transitions that contribute to XANES, additional peaks appear below the lowest absorption transition. These are attributed to core transitions from valence excited states. We next analyze the simulated O/N 2DXCS cross peaks of the three isomers of aminophenol. We show that the cross peaks carry information about the spatial localization of the corresponding valence states due to interference between the ground-state bleaching and excited-state absorption components of the signal. The cross peaks are sensitive to the relative position of the O and N atoms, in contrast to the N 1*s* XANES and diagonal N/N 2DXCS spectra of para- and ortho-aminophenol, which are quite similar to aniline, in accordance with the building-block principle.[1] Our results are finally summarized in Sec. V.

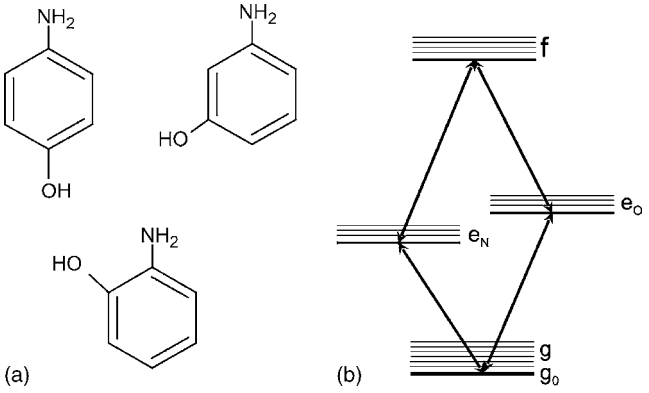

FIG. 2. (a) Para, meta, and ortho isomers of aminophenol. (b) Valence and core-excited states of aminophenol. g denotes states with no core electron excited (including the ground state g_0), e_j denotes states with one core-electron of type j excited, and f denotes states with two core-electrons excited.

II. SUM-OVER-STATES EXPRESSIONS FOR THE 2DXCS SIGNALS

We consider a four-wave-mixing experiment carried out using a sequence of four x-ray pulses (Fig. 1)

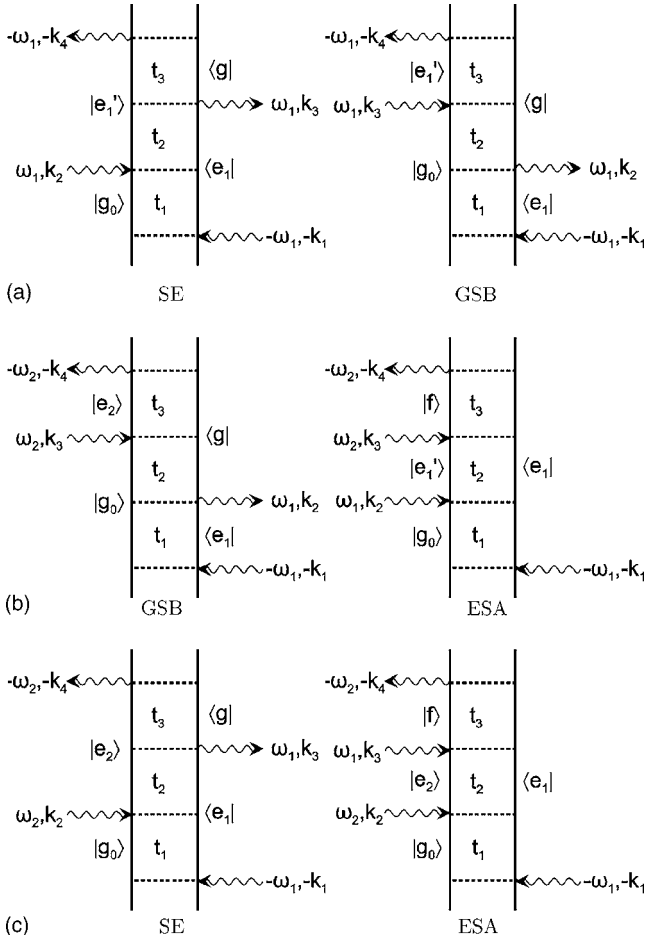

FIG. 3. Feynman diagrams representing (a) the SE and GSB contributions to the diagonal 2DXCS signal when only one core shell is in resonance [Eq. (10)], (b) the GSB and ESA contributions to the off-diagonal 2DXCS signal for the sequential two-color pulse configuration [Eq. (11)], and (c) the SE and ESA contributions to the off-diagonal 2DXCS signal for the nonsequential two-color pulse configuration.

$$E(\mathbf{r},t)=\sum_{j=1}^{4}[\mathcal{E}_j^{+}(t-\tau_j)e^{i\mathbf{k}_j\mathbf{r}-i\omega_j(t-\tau_j)}+\mathcal{E}_j^{-}(t-\tau_j)e^{-i\mathbf{k}_j\mathbf{r}+i\omega(t-\tau_j)}]. \quad (1)$$

Here $\mathcal{E}_j^{+}(t)$ is the complex temporal envelope $\boldsymbol{k}_j$ is the wave vector, and ω_j is the carrier frequency of the jth pulse. We consider ideal experiments with optically-thin samples and neglect the local field and the propagation effects. The interaction of the molecule with the first three pulses creates a polarization, which is heterodyne detected by overlapping the signal with the fourth pulse.

Assuming the dipole matter-field interaction $\hat{H}_{\mathrm{int}}=-\hat{V}E(\mathbf{r},t)$, the order-by-order contributions to the induced polarization are calculated by a time-dependent perturbative expansion in the field. In the phase-matching direction defined by $\boldsymbol{k}_I\equiv-\boldsymbol{k}_1+\boldsymbol{k}_2+\boldsymbol{k}_3$, the dominant contributions to the induced polarization come from specific third-order interactions with of the fields.[18] The signal is recorded as a function of the three delays t_1,t_2,t_3 between consecutive pulses (Fig. 1)

$$S_I^{(3)}(t_3,t_2,t_1)=\mathrm{Im}\int \mathrm{d}\boldsymbol{r}\int_{-\infty}^{\infty}\mathrm{d}\bar{\tau}_4 P^{(3)}(\boldsymbol{r},\bar{\tau}_4)\mathcal{E}_4^{*}(\bar{\tau}_4)e^{i\boldsymbol{k}_4\boldsymbol{r}-i\omega_4\bar{\tau}_4}. \quad (2)$$

We consider delays (1–10 fs) longer than the pulse durations (<1 fs), so that the system interacts with each pulse sequentially. We can thus use the result of Ref. 21 for a general sequential wave mixing and obtain (see also Appendix D)

$$S_I(t_3,t_2,t_1)=\mathrm{Im}\ R_I^{(3)}(t_3+t_2+t_1,t_2+t_1,t_1), \quad (3)$$

where

$$R_I^{(3)}(t_3+t_2+t_1,t_2+t_1,t_1)=i^3\langle[[[\hat{V}_4^{-}(t_3+t_2+t_1),\hat{V}_3^{+}(t_2+t_1)],\hat{V}_2^{+}(t_1)]\hat{V}_1^{-}(0)]\rangle \quad (4)$$

is the third-order molecular response function and

$$\hat{V}_j^{\pm}(\tau)=\int \mathrm{d}\bar{\tau}\mathcal{E}_j^{\pm}(\bar{\tau})\hat{V}(\bar{\tau}+\tau)e^{\mp i\omega_j\bar{\tau}}. \quad (5)$$

To calculate the response function [Eq. (4)], we expand $\hat{V}(\tau)$ in the molecular eigenstates Ψ_ν and eigenvalues E_ν,

$$\hat{V}(\tau)=\sum_{\mu,\nu}e^{i(\omega_{\mu\nu}-i\Gamma_{\mu\nu})\tau}V_{\mu\nu}\,|\Psi_\mu\rangle\langle\Psi_\nu|\ , \quad (6)$$

where $\omega_{\mu\nu}\equiv E_\mu-E_\nu$ is the frequency and Γ_μ is the dephasing rate of the transition between states ν and μ. Using Eq. (6), we recast Eq. (5) as

$$\hat{V}_j^{\pm}(\tau)=\sum_{\mu,\nu}\mathcal{E}_j^{\pm}(\omega_{\mu\nu}\mp\omega_j)e^{i\omega_{\mu\nu}\tau-\Gamma_{\mu\nu}\tau}V_{\mu\nu}\,|\Psi_\mu\rangle\langle\Psi_\nu|\ . \quad (7)$$

The dephasing time $1/\Gamma_{\mu\nu}$ given by the core-hole lifetime (~10 fs for K-edge transitions) is much longer than the pulse durations (<1 fs), thus the contribution of $\Gamma_{\mu\nu}$ to $\mathcal{E}(\omega)$ can be neglected. Since the duration of the x-ray pulse (~100 as) is much longer than its optical period (~4 as), $\mathcal{E}_j(\omega+\omega_j)$ vanishes for positive ω. In particular, $\hat{V}_j^{-}|\Psi_{g.s.}\rangle$ is zero. Only three terms then contribute to the commutator of Eq. (4),

$$\begin{aligned}R_I^{(3)}(t_3+t_2+t_1,t_2+t_1,t_1,0)&=i^3[\langle\hat{V}_1^{-}(0)\hat{V}_3^{+}(t_2+t_1)\hat{V}_4^{-}(t_3+t_2+t_1)\hat{V}_2^{+}(t_1)\rangle\\&+\langle\hat{V}_1^{-}(0)\hat{V}_2^{+}(t_1)\hat{V}_4^{-}(t_3+t_2+t_1)\hat{V}_3^{+}(t_2+t_1)\rangle\\&-\langle\hat{V}_1^{-}(0)\hat{V}_4^{-}(t_3+t_2+t_1)\hat{V}_3^{+}(t_2+t_1)\hat{V}_2^{+}(t_1)\rangle].\end{aligned} \quad (8)$$

The first two terms in Eq. (8) involve states with either none or only one core-electron excited and are denoted as the stimulated emission (SE) and ground-state bleaching (GSB) contributions, respectively. The third term involves states with two core-electrons excited and is referred to as the excited-states absorption (ESA) contribution. The corresponding double-sided Feynman diagrams are shown on Fig. 1.

We shall focus on the N and O K-edge 2DXCS signals of aminophenol (Fig. 2). The 2DXCS spectrum will be displayed as the Fourier transform of $S_I^{(3)}$ with respect to t_1 and t_3, holding t_2 fixed

$$S_I^{(3)}(\Omega_3,t_2,\Omega_1)=\int\int_0^{\infty}\mathrm{d}t_1\mathrm{d}t_3 S_I^{(3)}(t_3,t_2,t_1)e^{i\Omega_3t_3+i\Omega_1t_1}. \quad (9)$$

Since the pulse bandwidths (~10 eV for a 125 as pulse) are much smaller than the N and O K edges (~400 and ~535 eV, respectively) splitting, all three terms in Eq. (8) vanish unless either all carrier frequencies are tuned to the same type of core transitions (one-color) or two frequencies are tuned to one and the other two frequencies to the other type of core transition (two-color).

In a one-color experiment, all four pulse frequencies are tuned to either N or O core shell. We assume that after the first core electron is excited to a valence level, the relaxation energy of the remaining core electron is larger than the pulse bandwidth and the core transitions from a core-excited atom are off-resonant. Since, aminophenol has only one atom of each type, only the SE and GSB terms of Eq. (8) (Fig. 3) contribute to the response function [Eq. (A1)] and the signal is given by

$$\begin{aligned}S_{I,A}^{(3)}(\Omega_3,t_2,\Omega_1)=\mathrm{Re}\sum_{g,e_1,e_1'}&\frac{\mathcal{E}_1^{-}(\omega_{g_0e_1}+\omega_1)\mathcal{E}_1^{+}(\omega_{e_1g}-\omega_1)\mathcal{E}_1^{-}(\omega_{ge_1'}+\omega_1)\mathcal{E}_1^{+}(\omega_{e_1'g_0}-\omega_1)V_{g_0e_1}V_{e_1g}V_{ge_1'}V_{e_1'g_0}e^{-i\omega_{e_1'e_1}t_2-\Gamma_{e_1'e_1}t_2}}{(\Omega_1+\omega_{e_1g_0}+i\Gamma_{e_1g_0})(\Omega_3-\omega_{e_1'g}+i\Gamma_{e_1'g})}\\+\mathrm{Re}\sum_{g,e_1,e_1'}&\frac{\mathcal{E}_1^{-}(\omega_{g_0e_1}+\omega_1)\mathcal{E}_1^{+}(\omega_{e_1g}-\omega_1)\mathcal{E}_1^{-}(\omega_{ge_1'}+\omega_1)\mathcal{E}_1^{+}(\omega_{e_1'g_0}-\omega_1)V_{g_0e_1}V_{e_1g}V_{ge_1'}V_{e_1'g_0}e^{-i\omega_{gg_0}t_2-\Gamma_{gg_0}t_2}}{(\Omega_1+\omega_{e_1g}+i\Gamma_{e_1g})(\Omega_3-\omega_{e_1'g}+i\Gamma_{e_1'g})}.\end{aligned} \quad (10)$$

There are two possible two-color techniques. In the sequential configuration, the first two pulses are tuned to the same core transition and the other two are resonant with a different type (i.e., $\omega_1=\omega_2\neq\omega_3=\omega_4$). Only the GSB and ESA terms (Fig. 3) then contribute in this case to the response function [Eq. (A2)] and the signal is given by

$$S^{(3)}_{I,B}(\Omega_3,t_2,\Omega_1)=\mathrm{Re}\sum_{g,e_1,e_3}\frac{\mathcal{E}_1^-(\omega_{g_0e_1}+\omega_1)\mathcal{E}_1^+(\omega_{e_1g}-\omega_1)\mathcal{E}_3^-(\omega_{ge_3}+\omega_3)\mathcal{E}_3^+(\omega_{e_3g_0}-\omega_3)V_{g_0e_1}V_{e_1g}V_{ge_3}V_{e_3g_0}e^{-i\omega_{gg_0}t_2-\Gamma_{gg_0}t_2}}{(\Omega_1+\omega_{e_1g_0}+i\Gamma_{e_1g_0})(\Omega_3-\omega_{e_3g}+i\Gamma_{e_3g})}$$
$$-\mathrm{Re}\sum_{e_1,e_1',f}\frac{\mathcal{E}_1^-(\omega_{g_0e_1}+\omega_1)\mathcal{E}_3^-(\omega_{e_1f}+\omega_3)\mathcal{E}_1^+(\omega_{fe_1'}-\omega_{13})\mathcal{E}_1^+(\omega_{e_1'g_0}-\omega_1)V_{g_0e_1}V_{e_1f}V_{fe_1'}V_{e_1'g_0}e^{i\omega_{e_1e_1't_2}-\Gamma_{e_1e_1't_2}}}{(\Omega_1+\omega_{e_1g_0}+i\Gamma_{e_1g_0})(\Omega_3-\omega_{fe_1}+i\Gamma_{fe_1})}. \quad (11)$$

In the staggered configuration, the first and third pulses are tuned to one and the second and fourth to a different core transition (i.e., $\omega_1=\omega_3\neq\omega_2=\omega_4$). Only the SE and ESA terms (Fig. 3) then contribute to the response function [Eq. (A3)], and the signal is given by

$$S^{(3)}_{I,C}(\Omega_3,t_2,\Omega_1)=\mathrm{Re}\sum_{g,e_1,e_2}\frac{\mathcal{E}_1^-(\omega_{g_0e_1}+\omega_1)\mathcal{E}_1^+(\omega_{e_1g}-\omega_1)\mathcal{E}_2^-(\omega_{ge_2}+\omega_2)\mathcal{E}_2^+(\omega_{e_2g_0}-\omega_2)V_{g_0e_1}V_{e_1g}V_{ge_2}V_{e_2g_0}e^{-i\omega_{e_2e_1}t_2-\Gamma_{e_2e_1}t_2}}{(\Omega_1+\omega_{e_1g_0}+i\Gamma_{e_1g_0})(\Omega_3-\omega_{e_2g}+i\Gamma_{e_2g})}$$
$$-\mathrm{Re}\sum_{e_1,e_1',f}\frac{\mathcal{E}_1^-(\omega_{g_0e_1}+\omega_1)\mathcal{E}_2^-(\omega_{e_1f}+\omega_2)\mathcal{E}_1^+(\omega_{fe_2}-\omega_1)\mathcal{E}_2^+(\omega_{e_2g_0}-\omega_2)V_{g_0e_1}V_{e_1f}V_{fe_1'}V_{e_1'g_0}e^{i\omega_{e_1e_2t_2}-\Gamma_{e_1e_2}t_2}}{(\Omega_1+\omega_{e_1g_0}+i\Gamma_{e_1g_0})(\Omega_3-\omega_{fe_1}+i\Gamma_{fe_1})}. \quad (12)$$

Equations (10)–(12) reveal the dependence of 2DXCS on the pulse carrier frequencies ω_j; the t_1 and t_3 delays (through their Fourier conjugates Ω_1, Ω_3), and the second delay period t_2.

III. COMPUTATIONAL PROTOCOL

The dependence of the 2DXCS signal [Eqs. (10)–(12)] on the three excited-state manifolds (valence, singly core excited, and doubly core excited) makes its first-principles simulations particularly challenging. We use a simple approach originated in the early work of Nozieres and De Dominicus[19] and Mahan,[22] whereby the many-body interaction between the valence and core electrons is approximated by the classical Coulomb interaction. The wave functions describing states with no core hole (including the ground state) are factorized into the valence and core parts

$$\Psi_g(\boldsymbol{r}_1,\ldots,\boldsymbol{r}_N)\approx\psi_c(\boldsymbol{r}_1)\Phi_g(\boldsymbol{r}_2,\ldots,\boldsymbol{r}_N), \quad (13)$$

where we assume one core electron. Core-excited states Ψ_e are given by the eigenstates of a Hamiltonian describing $N+1$ valence electrons fully relaxed in the presence of the core-hole potential

$$\Psi_e(\boldsymbol{r}_1,\ldots,\boldsymbol{r}_N)\approx\tilde{\Phi}_e(\boldsymbol{r}_1,\ldots,\boldsymbol{r}_N). \quad (14)$$

The core transition frequencies are given by $\omega_{eg_0}\approx\tilde{E}_e-E_g$ and the dipole moment is calculated by neglecting the overlap between ψ_c and $\tilde{\Phi}_e$,

$$\langle\Psi_e|\hat{V}|\Psi_{g_0}\rangle\approx\int \mathrm{d}\boldsymbol{r}\mathrm{d}\boldsymbol{r}_1\ldots\mathrm{d}\boldsymbol{r}_N\tilde{\Phi}_e^*(\boldsymbol{r},\boldsymbol{r}_1,\ldots,\boldsymbol{r}_N)\times\hat{V}(\boldsymbol{r})\psi_c(\boldsymbol{r})\Phi_g(\boldsymbol{r}_1,\ldots,\boldsymbol{r}_N). \quad (15)$$

In the ECA, the core-hole potential is described by the Coulomb potential of a positive point charge located at the nuclei. The effect of this potential is equivalent to increasing the nuclear charge by one.[20,23] Thus, calculating singly core excited states within the ECA amounts to incrementing the charge of the corresponding nucleus by one, adding a valence electron, and performing *ab initio* calculations of the ground and valence excited states of the equivalent-core (or $N+1,Z_j+1$) molecule. Similarly, the states with two core electrons excited are given by the valence states of a second equivalent-core (or $N+2,Z_j+1,Z_{j'}+1$) molecule obtained by incrementing the charge of two nuclei by one and adding two valence electrons. Thus, within the ECA, all three excited-state manifolds can be calculated using the same *ab initio* approach. All necessary calculations can be performed with standard electronic-structure codes, where the nuclear charges and the number of electrons are parts of the input.

We next need to choose a level of theory to describe the valence excitations of the original and equivalent-core systems. In a previous simulation[12] we have used a simple approximation, whereby the transition frequencies are given by the difference in the KS orbital energies, and transition dipole moments are calculated using KS orbitals describing the promoted core electron. This model can be straightforwardly extended to include the effects of the valence electron relaxation by using Slater determinants made of KS orbitals. This model (referred to as DFT/ECA), previously used to simulate the x-ray Raman signal,[24] is extended here to include the doubly substituted determinants necessary to describe state with two core electrons excited. Within this model, eigenstates of the g manifold (states with no core electron excited) are given by

$$\Phi_g=\hat{\mathcal{A}}_N\phi_1(\boldsymbol{r}_1)\cdots\phi_p(\boldsymbol{r}_q)\cdots\phi_r(\boldsymbol{r}_s)\cdots\phi_N(\boldsymbol{r}_N), \quad (16)$$

$$E_g = \sum_{t=1}^{N} \epsilon_t + \epsilon_p + \epsilon_r - \epsilon_q - \epsilon_s, \tag{17}$$

where

$$\hat{\mathcal{A}}_N = \frac{1}{\sqrt{N!}} \sum_n^{N!} (-1)^{\sigma_n} \hat{P}_n \begin{pmatrix} 1, \ldots, N \\ n_1, \ldots, n_N \end{pmatrix}$$

is the antisymmetric sum over $N!$ permutations among N electron indices, ϵ_p and $\phi_p(\mathbf{r})$ are the eigenvalues and eigenfunction of the KS Hamiltonian of the original molecule

$$h_s = -\frac{1}{2}\nabla^2 + v_H + v_{xc} + \sum_{\alpha}^{N_{\text{nuc}}} \frac{Z_\alpha}{|\mathbf{r} - \mathbf{R}_\alpha|}. \tag{18}$$

The ground-state wave function Φ_{g_0} is given by the determinant with $p=q, r=s$, while valence excited states $\Phi_{g\neq g_0}$ are expressed by the singly substituted determinants $(p>N, q\leq N, r=s)$ and doubly substituted determinants $(p,r>N; q,s\leq N)$.

The e_j manifold eigenstates (states with jth core electron excited) are similarly given by

$$\Phi_{e_j} = \hat{\mathcal{A}}_{N+1} \tilde{\phi}_1(\mathbf{r}_1) \cdots \tilde{\phi}_p(\mathbf{r}_q) \cdots \tilde{\phi}_r(\mathbf{r}_s) \cdots \tilde{\phi}_{N+1}(\mathbf{r}_{N+1}), \tag{19}$$

$$E_{e_j} = \epsilon_j + \sum_{t=1}^{N+1} \tilde{\epsilon}_t + \tilde{\epsilon}_p - \tilde{\epsilon}_q + \tilde{\phi}_r - \tilde{\phi}_q, \tag{20}$$

where $\tilde{\epsilon}_p$ and $\tilde{\phi}_p(\mathbf{r})$ are the eigenvalues and eigenfunction of the KS Hamiltonian of equivalent-core molecule

$$\tilde{h}_s = \epsilon_j - \frac{1}{2}\nabla^2 + v_H + v_{xc} + \frac{Z_j + 1}{|\mathbf{r} - \mathbf{R}_\mathbf{n}|} + \sum_{\alpha\neq j}^{\text{nuclei}} \frac{Z_\alpha}{|\mathbf{r} - \mathbf{R}_\alpha|}. \tag{21}$$

The lowest core-state is given by the ground-state determinant $(p=q; r=s)$, while the valence excited states are represented by the singly substituted $(r=s; p>N q\leq N)$ and doubly substituted $(p, r>N+1; q, s\leq N+1)$ determinants. The ε_j parameter is chosen so that the difference between the ground-state energies of the original and equivalent-core molecules matches the frequency of the lowest core transition. The eigenstates of the f manifold (states with two core electrons excited) are similarly given by the ground and singly substituted determinants made up of the KS orbitals for the $N+2, Z_j+1, Z_{j'}+1$ system.

Upon substituting the single-determinant wave functions into Eq. (15) we obtain

$$\langle \Phi_{e_j} | \hat{V} | \Phi_g \rangle = \frac{1}{\sqrt{N!\,(N+1)!}} \sum_{n}^{(N+1)!} (-1)^{\sigma_n} \hat{P}_n \begin{pmatrix} 1, \ldots, N+1 \\ n_1, \ldots, n_{N+1} \end{pmatrix} \times \langle \tilde{\phi}_{n_1} | \phi_1 \rangle \cdots \langle \tilde{\phi}_{n_N} | \phi_N \rangle \langle \tilde{\phi}_{n_{N+1}} | \hat{\mu} | \phi_n \rangle, \tag{22}$$

the transition frequencies are

$$\omega_{e_j g} = \epsilon_j + \sum_{i=1}^{N+1} \tilde{\epsilon}_i + \tilde{\epsilon}_p - \tilde{\epsilon}_q - \sum_{i=1}^{N} \epsilon_i - \epsilon_p + \epsilon_q. \tag{23}$$

Similar expressions are used to calculate $e_j - f$ transition frequencies and matrix elements.

Adopting the same atomic basis set χ_μ for all equivalent-core molecules, these matrix elements can be easily calculated using the orbital coefficients $C_{p\mu}$ and matrix elements of the dipole operator, which are provided by the electronic structure code

$$\langle \tilde{\phi}_{p_1} | \phi_p \rangle = \sum_{\mu,\nu} \tilde{C}^*_{p_1\mu} C_{p\nu} \int \mathrm{d}\mathbf{r} \chi_\mu(\mathbf{r}) \chi_\nu(\mathbf{r}), \tag{24}$$

$$\langle \tilde{\phi}_{pN+1} | \hat{\mu} | \phi_n \rangle = \sum_{\mu,\nu} \tilde{C}^*_{p_1\mu} C_{n\nu} \int \mathrm{d}\mathbf{r} \chi_\mu(\mathbf{r}) \hat{\mu} \chi_\nu(\mathbf{r}). \tag{25}$$

In summary, simulation of 2DXCS signals involves ground-state density functional theory calculations of the original and equivalent-core molecules. Given the molecular orbital coefficients and the dipole matrix elements provided by the electronic structure code, the four sets of the transition frequencies and matrix elements are calculated according to Eqs. (22)–(25). The 2DXCS signal is finally obtained using Eqs. (10)–(12).

Equation (22) can be easily generalized to include excited states represented by a linear combination of the determinants rather than one determinant. In particular, time-dependent density functional theory (TDDFT) provides excellent accuracy for valence transitions at a moderate computational cost. TDDFT within the ECA has already been applied to calculate shake-up[25] and XANES spectra.[26,27] We have recently extended the ECA/TDDFT approximation to describe valence to core transitions in simulations of the x-ray Raman signals.[28] However, unlike XANES or Raman techniques, 2DXCS involves transitions to doubly core excited states. With the ECA, such states correspond to valence excited transitions that involve two electrons. For example, the second term in Eq. (11) involves transitions from a singly core excited state to a doubly core excited state. Within the ECA, the latter correspond to a valence state with two electrons excited. Such states are not included in TDDFT with existing, frequency-independent adiabatic approximations for the exchange-correlation kernel.[29] However, the simpler determinant-based model adapted here allows us to describe such states approximately using the doubly substituted determinants.

IV. NUMERICAL SIMULATIONS

In all calculations presented below, we used the KS orbitals obtained with Becke's three-parameter exchange-correlation functional[30] and the 6–311G** (Ref. 31) set of Gaussian-type atomic orbitals. The orbitals and orbital energies were obtained with the GAUSSIAN 03 program.[32] ε_N and ε_O were chosen so that the lowest N $1s$ and O $1s$ transition frequencies match the experimental values of 400.7 (Ref. 33) and 534.9 eV,[34] respectively. We assumed rectangular pulse envelopes $\mathcal{E}_j(\omega)$ of 10 eV width around the carrier frequen-

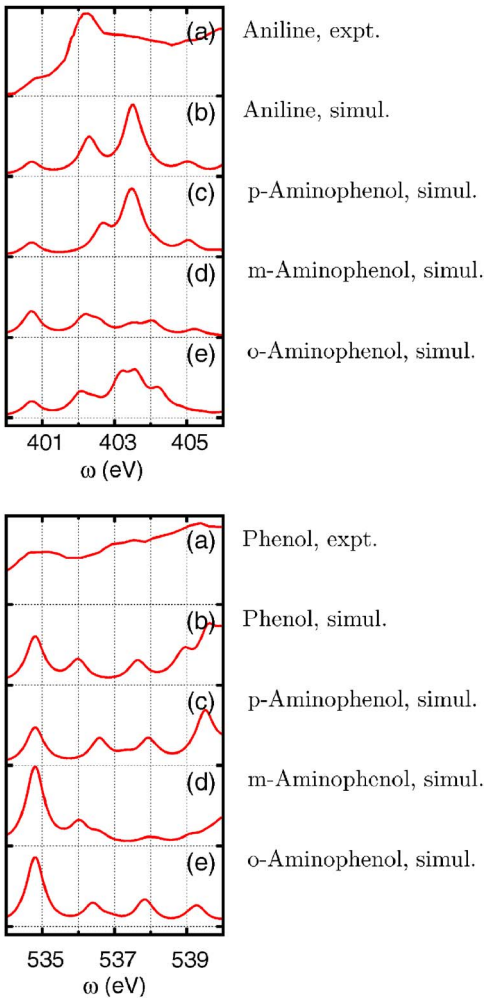

FIG. 4. (Color online) Comparison between the experimental and simulated N 1*s* (upper panel) and O 1*s* (lower panel) XANES of aniline, phenol, and the isomers of aminophenol. Experimental spectra are taken from Refs. 34 (aniline) and 33 (phenol).

cies [i.e., $\mathcal{E}_j(\omega)=1$ for $|\omega-\omega_j|\leq 5$ eV and zero otherwise]. This implies truncating the sums at the equivalent-core states whose energies are higher than 5 eV above the ground state. The same dephasing rate $\Gamma_{\mu\nu}=0.3$ eV was assumed for all transitions below the ionization edge. Note that with the chosen bandwidth, only states below the ionization edge contribute to the 2DXCS signal; transitions to continuum were neglected.

The calculated core-transition accuracy depends on how well the equivalent-core approximation describes the core potential as well as on the level of quantum chemistry employed to describe the electronic states of the equivalent-core molecules. The effect of these approximations on both the transition energies (peak positions) and matrix elements (peak intensities) can be evaluated by comparison with experiment. Figure 4 compares the calculated and experimental XANES for aniline, phenol, and the three isomers of aminophenol. The experimental N 1*s* XANES of anline[34] features three pre-edge peaks at 400.7 (weak), 402.2 (strong), and 404.0 (strong). The simulation reproduces the splittings between the peaks, however, underestimates the intensity of the second peak. The experimental O 1*s* XANES of phenol[33]

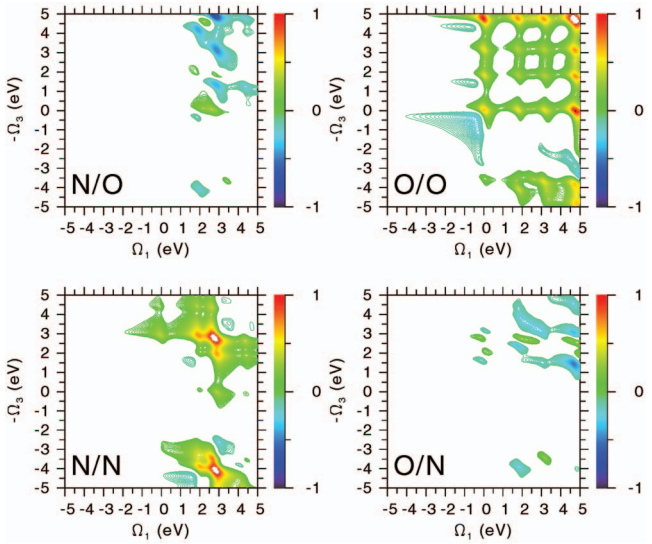

FIG. 5. (Color) The four regions of the simulated 2DXCS signal [Eqs. (10) and (11)] of para-aminophenol. $t_2=0$. Values of Ω_1 and Ω_3 are given relatively to the corresponding absorption edge (400.7 eV for N 1s and 534.9 eV for O 1*s* transitions.

features three pre-edge peaks of increasing intensity at 534.9, 537.2, and 539.4 eV. The simulated O 1*s* XANES consists of four peaks at 534.9, 537.0, 538.1, and 539.2 eV, reproducing the positions and intensities of the first and third experimental peaks, but underestimating the intensity of the second peak.

Figure 5 shows the 2DXCS spectrum of para-aminophenol in the N/N and O/O diagonal regime and N/O and O/N cross-peak regime. At $t_2=0$, the GSB and SE terms contributing to the diagonal N/N and O/O 2DXCS signals [Eq. (10)] are equal and result in a strong positive signal with weak negative tails. The N/O and O/N cross peaks are much weaker as a result of the interference between the GSB and ESA terms [Eq. (11)]. Only the 2DXCS obtained in the sequential two-color configuration is shown, since the nonsequential configuration [Eq. (12)] yields the essentially identical signal at $t_2=0$.

The N/N signal of Fig. 5 is repeated in Fig. 6, where we also show the XANES spectra to help assign the peaks. As

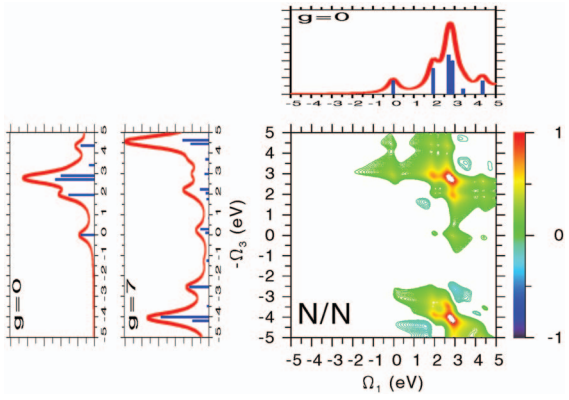

FIG. 6. (Color) Simulated diagonal N/N 2DXCS signal of para-aminophenol. $t_2=0$. Insets show simulated N 1*s* XANES from the ground and valence excited states contributing to the N/N 2DXCS spectrum. Values of Ω_1 and Ω_3 are given relatively to the N 1*s* absorption edge (400.7 eV).

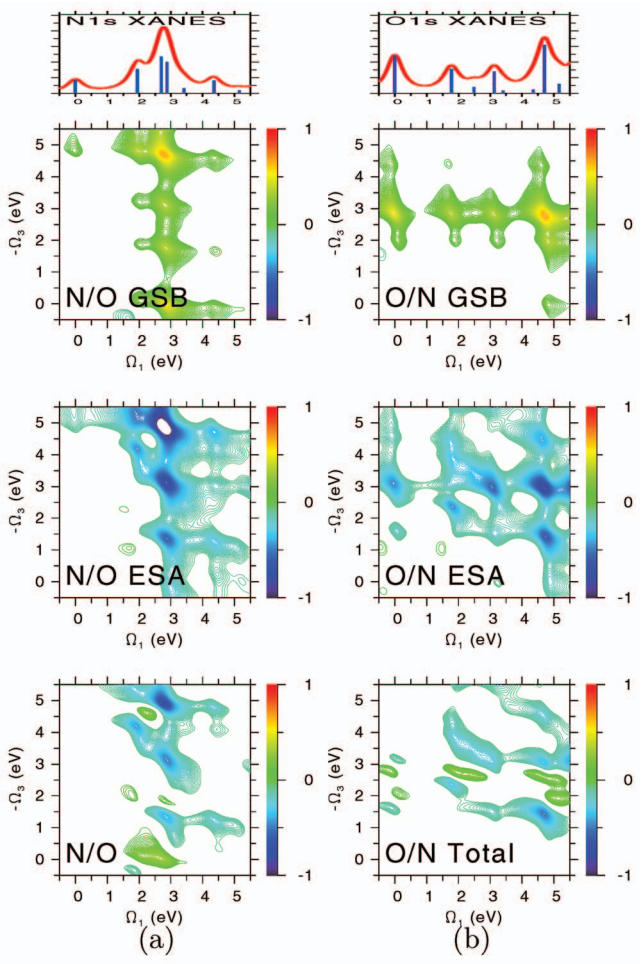

FIG. 7. (Color) (a) Simulated N 1*s* XANES, the GSB and ESA components, and the total N/O 2DXCS cross peak and (b) stimulated O 1*s* XANES, the GSB and ESA components, and total O/N cross peak of para-aminophenol. $t_2=0$. Values of Ω_1 and Ω_3 are given relatively to the corresponding absorption edge (400.7 eV for N 1*s* and 534.9 eV for O 1*s* transitions.)

shown in Appendix B, there are two types of contributions to the diagonal signal. The first arising from transitions between the ground state and core-excited states can be factorized into the product of the linear absorption spectra. The corresponding peaks located in the $\Omega_3 \geq 0$ half of the correlation spectrum can be identified by comparing with the linear absorption spectra. The other contribution arises from transitions between the valence-excited and core-excited states. The corresponding peaks can be identified by their position in the $\Omega_3 < 0$ half of the spectrum. The strong feature at $\Omega_3 \approx -4$ eV appears due to the N 1*s* absorption from valence state.

Figure 7 shows the GSB and ESA components and the total N/O and O/N 2DXCS cross peaks of para-aminophenol. As shown in Appendix C, if the two types of core transition are independent, we expect both terms to be approximately equal to the product of the linear absorption of each type. Both N/O and O/N pulse configurations yield strong individual GSB and ESA contributions, however, the total cross peak is much weaker due to interference. In a heterodyne measurement, such as 2DXCS it is possible to observe the real part of the response function by varying the relative phases of the incoming pulse. The real, imaginary, and absolute value N/O signals are shown in the supplementary material.[35]

Figure 8 shows the simulated N 1*s* XANES, N/N 2DXCS, and N/O 2DXCS spectra of aniline, para-, and ortho-aminophenol. The corresponding calculated N 1*s* XANES signals of aniline, para-, and ortho-aminophenol are remarkably similar. This is in accordance with building-block principle of XANES spectroscopy, which states that the contributions of multiple core shells are additive.[1] Indeed, the XANES spectra of the amine N weakly depend on whether the hydroxyl group is in the para or ortho position, or is not present at all. The N/N 2DXCS signal is similarly insensitive to whether the hydroxyl group is in the para or the ortho position or is not present at all. As discussed earlier, the major features above the lowest absorption transition arise form the same transitions that contribute to XANES. The similarity of the N/N 2DXCS signal below the lowest absorption transition shows that the transitions from valence excited states are as well insensitive to the position of the hydroxyl group. The situation is markedly different for the N/O 2DXCS cross peak as the effect of the N 1*s* transitions on the O 1*s* absorption strongly depends on the relative position of two atoms. For example, the contribution of the lowest O 1*s* excited state is much stronger in the ortho isomer leading to a strong 2DXCS cross peak at $\Omega_3=0$. In contrast, the 2DXCS cross peak of para-aminophenol lacks strong features at near the O 1*s* absorption edge, but has two distinctive peaks at $\Omega_3 \sim 3$ and 5 eV.

V. CONCLUSIONS

We have simulated two-dimensional x-ray correlation spectra obtained from the $\boldsymbol{k}_I=-\boldsymbol{k}_1+\boldsymbol{k}_2+\boldsymbol{k}_3$ phase-matching component of the sequential coherent all-x-ray four-wave-mixing signal. The diagonal part of the 2DXCS spectrum is obtained with a one-color pulse configuration when all carrier frequencies are resonant with a given type of core transitions. Off-diagonal cross peaks are obtained with a two-color (either sequential or nonsequential) configuration where two pulses are tuned to one and the other two pulses are tuned to another type of core transition. Various regions of the 2DXCS spectrum probe different types of interactions between transitions and provide complimentary information about the electronic states of the molecule.

Closed-form expressions for the 2DXCS signals obtained in three possible pulse configurations were derived using an expansion over molecular eigenstates. We have implemented a simple scheme for calculating these states whereby the valence and core-excited states are represented by the ground state, singly and doubly substituted Kohn–Sham determinants of the original and equivalent-core molecules. Comparison of the calculated XANES spectra of aniline and phenol with experiment showed that our computational algorithm reproduces the positions of core transitions with significant intensities, but underestimates the intensities of some peaks.

The simulated diagonal N/N 2DXCS spectrum of para-aminophenol contains contributions of transitions from

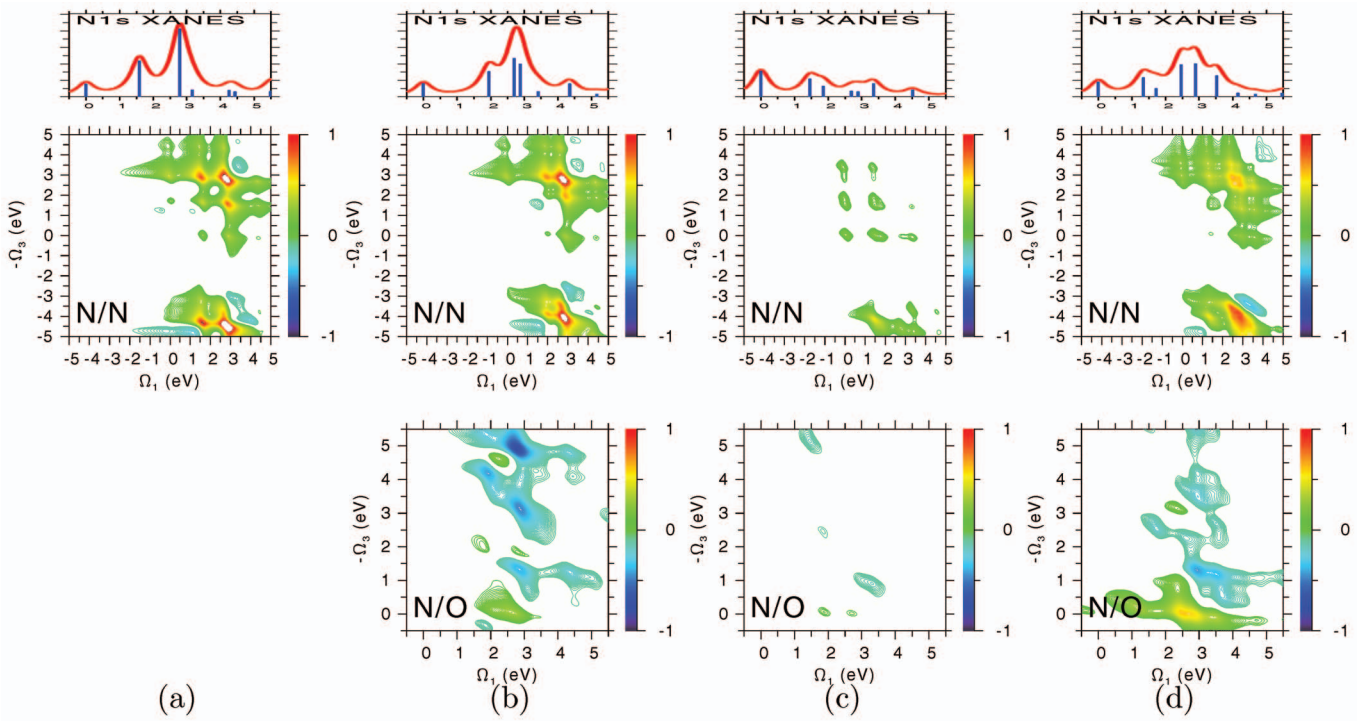

FIG. 8. (Color) Simulated N 1*s* XANES (upper panel), diagonal N/N 2DXCS signal (center panel), and N/O 2DXCS cross peaks (lower panel) of (a) aniline, (b) para-, (c) meta-, and (d) ortho-aminophenol. Values of Ω_1 and Ω_3 are given relatively to the corresponding absorption edge (400.7 eV for N 1*s* and 534.9 eV for O 1*s* transitions.)

valence-excited to core-excited states, in addition to the transitions from ground to core-excited states already visible in XANES. The corresponding peaks can be identified by their positions below the lowest ground-state XANES along the Ω_3 axis. The diagonal 2DXCS signal thus provides information similar to the one obtained in the resonant x-ray emission spectroscopy, however, transitions from multiple core-excited states included in the bandwidth are observed simultaneously.

The N/O and O/N 2DXCS cross peaks of para-aminophenol consist of two strong contributions, whose interference results in a much weaker total signal. Previously, we had demonstrated that the cross peaks provide information about the core excited-state wave functions beyond the dipole coupling available in XANES.[12] In particular, we showed that a strong contribution to XANES but weak 2DXCS cross peak indicates localization of the promoted core electron to the atom in resonance. Alternatively, a weak XANES contribution accompanied with a strong 2DXCS cross peak indicated the delocalization of the promoted core electron over the two atoms whose core shells are in resonance. The simulations of the cross peaks in the three isomers of aminophenol presented here showed that they are also sensitive to the relative position of the amine and hydroxyl groups, even if XANES or diagonal 2DXCS are not. The 2DXCS cross peaks thus provide further insights into the molecular and electronic structure than available in XANES or resonant XES.

The proposed 2DXCS measurements are beyond the capabilities of existing x-ray sources. While the HHG is capable of producing spatially coherent attosecond pulses, its brilliance is insufficient to detect the four-wave mixing signal. We estimated that there is only one generated photon per 10^{15} incoming photons in the fully resonant four-wave mixing measurement.[12] Even with the XFEL capability of generating 10^{13} photons per pulse, high repetition rates and long acquisition times will be necessary to make the experiment feasible. Other experimental challenges include reducing the duration of the XFEL pulse and generating multiple pulses with controlled timing and phase.

Predicting and interpreting the 2DXCS spectra will provide a critical test for electron structure calculations and should stimulate the development of highly accurate methods for core transitions. The singly and doubly substituted Kohn–Sham determinants employed in this work are sufficient for the qualitative analysis of the 2DXCS spectra, but do not capture the subtle details of many-electron interactions which can be elucidated by 2DXCS spectroscopy. TDDFT, for example, is capable of describing these interactions, yet robust enough to allow treatment of relatively large molecules. However, current implementations of TDDFT use a frequency-independent kernels and do not reproduce excited states with two electron excited. These states give rise to the ESA part of the 2DXCS cross peak above the lowest transitions and are necessary to reproduce the cross peak in this region. Reproducing the experimental 2DXCS cross peaks should provide a stringent test for frequency-dependent TDDFT or other methods for excited states of two-electron character.

ACKNOWLEDGMENTS

We thank the anonymous referee for pointing out the dependence of the 2DXCS cross peaks on the distance be-

tween the core shells. The support from Chemical Sciences, Geosciences and Biosciences Division, Office of Basic Energy Sciences, Office of Science, U.S. Department of Energy is gratefully acknowledged.

APPENDIX A: SUM-OVER-STATE EXPRESSIONS FOR $R_I^{(3)}$

In a one-color pulse configuration, only the SE and GSB terms [Fig. 3(a)] contribute if only one atom of the given type is present. The response function is given by

$$R_{I,A}^{(3)}(t_3,t_2,t_1) = i^3 \sum_{g,e_1,e_1'} \mathcal{E}_1^-(\omega_{g_0e_1}+\omega_1)\mathcal{E}_1^+(\omega_{e_1g}-\omega_1)\mathcal{E}_1^-(\omega_{ge_1'}+\omega_1)\mathcal{E}_1^+(\omega_{e_1'g_0}-\omega_1)V_{g_0e_1}V_{e_1g}V_{ge_1'}V_{e_1'g_0}$$
$$\times e^{i(\omega_{e_1g_0}-i\Gamma_{e_1g_0})t_1+i(\omega_{e_1'e_1}-i\Gamma_{e_1'e_1})t_2-i(\omega_{e_1'g}-i\Gamma_{e_1'g})t_3} + i^3 \sum_{g,e_1,e_1'} \mathcal{E}_1^-(\omega_{g_0e_1}+\omega_1)\mathcal{E}_1^+(\omega_{e_1g}-\omega_1)\mathcal{E}_1^-(\omega_{ge_1'}-\omega_1)$$
$$\times \mathcal{E}_1^+(\omega_{e_1'g_0}-\omega_1)V_{g_0e_1}V_{e_1g}V_{ge_1'}V_{e_1'g_0}e^{i(\omega_{e_1g_0}-i\Gamma_{e_1g_0})t_1+i(\omega_{gg_0}-i\Gamma_{gg_0})t_2-i(\omega_{e_1'g}-i\Gamma_{e_1'g})t_3}. \quad \text{(A1)}$$

In a sequential two-color pulse configuration, only the GSB and ESA terms contribute [Fig. 3(b)] and the response function is given by

$$R_{I,B}^{(3)}(t_3,t_2,t_1) = i^3 \sum_{g,e_1,e_3} \mathcal{E}_1^-(\omega_{g_0e_1}+\omega_1)\mathcal{E}_1^+(\omega_{e_1g}-\omega_1)\mathcal{E}_3^-(\omega_{ge_3}+\omega_3)\mathcal{E}_3^+(\omega_{e_3g_0}-\omega_3)V_{g_0e_1}V_{e_1g}V_{ge_3}V_{e_3g_0}$$
$$\times e^{i(\omega_{e_1g_0}-i\Gamma_{e_1g_0})t_1+i(\omega_{gg_0}-i\Gamma_{gg_0})t_2-i(\omega_{e_3g}-i\Gamma_{e_3g})t_3} - i^3 \sum_{e_1,e_1',f} \mathcal{E}_1^-(\omega_{g_0e_1}+\omega_1)\mathcal{E}_3^-(\omega_{e_1f}+\omega_3)\mathcal{E}_3^+(\omega_{fe_1'}-\omega_3)\mathcal{E}_1^+(\omega_{e_1'g_0}$$
$$-\omega_1)V_{g_0e_1}V_{e_1f}V_{fe_1'}V_{e_1'g_0}e^{i(\omega_{e_1g_0}-i\Gamma_{e_1g_0})t_1+i(\omega_{e_1e_1'}-i\Gamma_{e_1e_1'})t_2-i(\omega_{fe_1}-i\Gamma_{fe_1})t_3}. \quad \text{(A2)}$$

In a nonsequential two-color pulse configuration, only the SE and ESA terms contribute [Fig. 3(c)] and the response function is given by

$$R_{I,C}^{(3)}(t_3,t_2,t_1) = i^3 \sum_{g,e_1,e_2} \mathcal{E}_1^-(\omega_{g_0e_1}+\omega_1)\mathcal{E}_1^+(\omega_{e_1g}-\omega_1)\mathcal{E}_2^-(\omega_{ge_2}+\omega_2)\mathcal{E}_2^+(\omega_{e_2g_0}-\omega_2)V_{g_0e_1}V_{e_1g}V_{ge_2}V_{e_2g_0}$$
$$\times e^{i(\omega_{e_1g_0}-i\Gamma_{e_1g_0})t_1+i(\omega_{e_1e_2}-i\Gamma_{e_1e_2})t_2-i(\omega_{e_2g}-i\Gamma_{e_2g})t_3} - i^3 \sum_{e_1,e_2,f} \mathcal{E}_1^-(\omega_{g_0e_1}+\omega_1)\mathcal{E}_2^-(\omega_{e_1f}+\omega_2)\mathcal{E}_1^+(\omega_{fe_2}-\omega_1)$$
$$\times \mathcal{E}_2^+(\omega_{e_2g_0}-\omega_2)V_{g_0e_1}V_{e_1f}V_{fe_2}V_{e_2g_0}e^{i(\omega_{e_1g_0}-i\Gamma_{e_1g_0})t_1+i(\omega_{e_1e_2}-i\Gamma_{e_1e_2})t_2-i(\omega_{fe_1}-i\Gamma_{fe_1})t_3}. \quad \text{(A3)}$$

APPENDIX B: ORIGIN OF THE DIAGONAL 2DXCS SIGNAL

At $t_2=0$, the SE and GSB terms contributing to the diagonal signal [Eq. (10)] become equal and $S_{I,A}^{(3)}$ can be recast into

$$S_{I,A}^{(3)}(\Omega_3,0,\Omega_1) = 2S_1^{(1)}(-\Omega_1)S_1^{(1)}(\Omega_3) + 2\sum_{g\neq g_0,e_1} \frac{\mathcal{E}_1^-(\omega_{g_0e_1}+\omega_1)\mathcal{E}_1^+(\omega_{e_1g}-\omega_1)V_{g_0e_1}V_{e_1g}}{\Omega_1+\omega_{e_1g_0}+i\Gamma_{e_1g_0}}$$
$$\times \sum_{e_1'} \frac{\mathcal{E}_1^-(\omega_{ge_1'}+\omega_1)\mathcal{E}_1^+(\omega_{e_1'g_0}-\omega_1)V_{ge_1'}V_{e_1'g_0}}{\Omega_3-\omega_{e_1'g}+i\Gamma_{e_1'g}}, \quad \text{(B1)}$$

where we have separated the summation over states with no core electron excited (g) into terms involving only the ground state (g_0) and terms include also the valence excited states ($g\neq g_0$), and

$$S_j^{(1)}(\Omega) = \sum_{e_j} \frac{|\mathcal{E}_j^2(\omega_{e_jg_0}-\omega_j)V_{e_jg_0}|^2}{\Omega-\omega_{e_jg_0}+i\Gamma_{e_jg_0}}. \quad \text{(B2)}$$

Thus, we identify two types of contributions to the diagonal 2DXCS signal. The first arises from the same transitions that contribute to the XANES and is given by the product of XANES signals along the Ω_1 and Ω_3 axes. The other arises from transitions form the valence to core excited states.

APPENDIX C: ORIGIN OF THE OFF-DIAGONAL 2DXCS SIGNAL

The off-diagonal signal [Eq. (11)] is given by the difference between the GSB and ESA terms

$$S_{I,B}^{(3)}(\Omega_3,t_2,\Omega_1) = S_{I,B}^{\mathrm{GSB}}(\Omega_3,t_2,\Omega_1) - S_{I,B}^{\mathrm{ESA}}(\Omega_3,t_2,\Omega_1). \quad \text{(C1)}$$

If there is no valence excited state with a significant dipole coupling to both types of the core transitions, then

$$V_{e_1g}V_{ge_3} \approx V_{e_1g_0}V_{g_0e_3}\delta_{gg_0} \tag{C2}$$

and we can recast the GSB term as

$$\begin{aligned} S_{I,B}^{\mathrm{GSB}}(\Omega_3,t_2,\Omega_1) &= \sum_{e_1} \frac{\mathcal{E}_1^-(\omega_{g_0e_1}+\omega_1)\mathcal{E}_1^+(\omega_{e_1g_0}-\omega_1)V_{g_0e_1}V_{e_1g_0}}{\Omega_1+\omega_{e_1g_0}+i\Gamma_{e_1g_0}} \\ &\times \sum_{e_3} \frac{\mathcal{E}_3^-(\omega_{g_0e_3}+\omega_3)\mathcal{E}_3^+(\omega_{e_3g_0}-\omega_3)V_{g_0e_3}V_{e_3g_0}}{\Omega_3-\omega_{e_3g}+i\Gamma_{e_3g}} \\ &= S_1^{(1)}(-\Omega_1)S_3^{(1)}(\Omega_3). \end{aligned} \tag{C3}$$

If the core transitions of one type are not effected by the presence of a core hole of a different type, then

$$V_{e_1f}V_{fe_1'} \approx V_{g_0e_3}V_{e_3g_0}\delta_{e_1e_1'},$$

$$\omega_{e_1f} \approx \omega_{g_0e_3} \tag{C4}$$

and we can recast the ESA term into (for $t_2 \ll 1/\Gamma_{e_1e_1}$)

$$\begin{aligned} S_{I,B}^{\mathrm{ESA}}(\Omega_3,t_2,\Omega_1) &= \sum_{e_1} \frac{\mathcal{E}_1^-(\omega_{g_0e_1}+\omega_1)\mathcal{E}_1^+(\omega_{e_1g}-\omega_1)V_{g_0e_1}V_{e_1g_0}}{\Omega_1+\omega_{e_1g_0}+i\Gamma_{e_1g_0}} \\ &\times \sum_{e_3} \frac{\mathcal{E}_3^-(\omega_{g_0e_3}+\omega_3)\mathcal{E}_3^+(\omega_{e_3g_0}-\omega_3)V_{g_0e_3}V_{e_3g_0}}{\Omega_3-\omega_{e_3g}+i\Gamma_{e_3g}} e^{-\Gamma_{e_1e_1}t_2} \\ &= S_1^{(1)}(-\Omega_1)S_3^{(1)}(\Omega_3). \end{aligned} \tag{C5}$$

Thus, if two types of core transitions are independent [i.e., conditions (C2) and (C4) are satisfied] then both GSB and ESA terms factorize into the product of the linear absorptions of each type and the total off-diagonal signal given by their difference vanishes.

APPENDIX D: SPATIAL DEPENDENCE OF 2DXCS SIGNALS

In the derivation of Eq. (3), we have assumed the dipole matter-field interaction. The quadrupole and higher-order terms are small since the spatial extent of the N $1s$ core orbital (<0.3 A) is much smaller then the wavelength of the x-ray pulse tuned to the N $1s$ transitions (~ 30 A). However, if multiple, spatially separated, core shells contribute to the 2DXCS signal, one must take into account the variation in the field amplitude due to the difference in the positions of the core shells.

Within the dipole approximation, the dependence of the individual signal on positions of the core shells is given by

$$\begin{aligned} S_I(t_3,t_2,t_1) &= \mathrm{Im}\, R_I^{(3)}(t_3+t_2+t_1,t_2+t_1,t_1) \\ &\times e^{-i\boldsymbol{k}_1\boldsymbol{r}_1+i\boldsymbol{k}_2\boldsymbol{r}_2+i\boldsymbol{k}_3\boldsymbol{r}_3-i\boldsymbol{k}_4\boldsymbol{r}_4}, \end{aligned} \tag{D1}$$

where $\boldsymbol{r}_j$ is the absolute position (in the laboratory frame) of the core shell interacting with pulse j.

The 2DXCS signal is measured under the phase matching condition ($-\boldsymbol{k}_1+\boldsymbol{k}_2+\boldsymbol{k}_3-\boldsymbol{k}_4=0$). It thus depends solely on the relative positions of the core shells with the given molecule

$$e^{-i\boldsymbol{k}_1\boldsymbol{r}_1+i\boldsymbol{k}_2\boldsymbol{r}_2+i\boldsymbol{k}_3\boldsymbol{r}_3-i\boldsymbol{k}_4\boldsymbol{r}_4} = e^{-i\boldsymbol{k}_1\boldsymbol{R}_1+i\boldsymbol{k}_2\boldsymbol{R}_2+i\boldsymbol{k}_3\boldsymbol{R}_3-i\boldsymbol{k}_4\boldsymbol{R}_4}, \tag{D2}$$

where $\boldsymbol{R}_j$ is the positions of the core shells relative to the molecular center of mass. Thus, if only one core shell contributes to the 2DXCS signal (e.g., the diagonal 2DXCS signal of aminophenol), then total signal is independent of the core shell position.

If two core shells contribute to the 2DXCS signal (e.g., cross peaks), then the signal dependence on the positions of the core shells is given by

$$e^{i(\boldsymbol{k}_2-\boldsymbol{k}_1)(\boldsymbol{R}_1-\boldsymbol{R}_2)} = e^{i2\pi q(L/\lambda)\cos\theta}, \tag{D3}$$

where θ is the angle between the vectors $\boldsymbol{k}_2-\boldsymbol{k}_1$, $\boldsymbol{R}_1-\boldsymbol{R}_2$, $q=|\boldsymbol{k}_2-\boldsymbol{k}_1|/|\boldsymbol{k}_1|$, and L is the distance between the two core shells contributing to the signal. Here θ depends on the orientation of the molecule in the laboratory frame and q ($0 \le q \le 2$) depends on the pulse configuration.

In an oriented sample, this factor is identical for all molecules and the dependence of the total 2DXCS cross peaks on the distance between the core shells is given by a constant factor $e^{i2\pi q(L/\lambda)\cos\theta}$. In an ensemble of randomly oriented molecules, the total 2DXCS signal is obtained by averaging over all possible molecular orientations and its dependence on the distance between is the two core shells is given by

$$\frac{1}{2}\int_0^\pi \sin\theta \mathrm{d}\theta e^{i2\pi(qL/\lambda)\cos\theta} = \mathrm{sinc}(2\pi qL/\lambda). \tag{D4}$$

The distance between the N and O atoms is 2.5 A in para-aminophenol. Assuming the orthogonal pulse configuration ($q \approx 1.5$), we obtain

$$\langle e^{i(\boldsymbol{k}_2-\boldsymbol{k}_1)(\boldsymbol{R}_1-\boldsymbol{R}_2)}\rangle \approx \mathrm{sinc}(\pi/4) \approx 0.9. \tag{D5}$$

The dependence of the total 2DXCS signal of aminophenol on the distance between the core shells can thus be neglected. It must, however, be taken into account in the 2DXCS cross peaks on the distance between the core shells must, however, be taken into account in the simulations of the 2DXCS spectra of large molecules, as cross peaks between well-separated core shells may vanish.

[1] J. Stohr, *NEXAFS Spectroscopy* (Springer, New York, 1996).
[2] F. Raksi, K. R. Wilson, Z. M. Jiang, A. Ikhlef, C. Y. Cote, and J. C. Kieffer, J. Chem. Phys. **104**, 6066 (1996).
[3] I. V. Tomov, D. A. Oulianov, P. L. Chen, and P. M. Rentzepis, J. Phys. Chem. B **103**, 7081 (1999).
[4] L. X. Chen, W. J. H. Jager, G. Jennings, D. J. Gosztola, A. Munkholm, and J. P. Hessler, Science **292**, 262 (2001).
[5] M. Saes, C. Bressler, R. Abela, D. Grolimund, S. L. Johnson, P. A. Heimann, and M. Chergui, Phys. Rev. Lett. **90**, 047403 (2003).
[6] C. Bressler and M. Chergui, Chem. Rev. **104**, 1781 (2004).
[7] P. H. Bucksbaum, Science **317**, 766 (2007).
[8] E. Goulielmakis, V. S. Yakovlev, A. L. Cavalieri, M. Uiberacker, V. Pervak, A. Apolonski, R. Kienberger, U. Kleineberg, and F. Krausz, Science **317**, 769 (2007).
[9] H. Kapteyn, O. Cohen, I. Christov, and M. Murnane, Science **317**, 775 (2007).
[10] A. A. Zholents and W. M. Fawley, Phys. Rev. Lett. **92**, 224801 (2004).
[11] R. Ernst, G. Bodenhausen, and A. Wokaun, *Principles of Nuclear Mag-*

netic Resonance in One and Two Dimensions (Clarendon, Oxford, 1987).
[12] I. V. Schweigert and S. Mukamel, Phys. Rev. Lett. **99**, 163001 (2007).
[13] S. Tanaka and S. Mukamel, J. Chem. Phys. **116**, 1877 (2002).
[14] S. Mukamel, Phys. Rev. B **72**, 235110 (2005).
[15] J. Jeener, B. H. Meier, P. Bachmann, and R. R. Ernst, J. Chem. Phys. **71**, 4546 (1979).
[16] S. Mukamel and R. Hochstrasser, Chem. Phys. **266**, 135 (2001).
[17] S. Mukamel, Annu. Rev. Phys. Chem. **51**, 691 (2000).
[18] S. Mukamel, *Principles of Nonlinear Optical Spectroscopy* (Oxford University Press, New York, 1995).
[19] P. Nozieres and C. DeDominicus, Phys. Rev. **178**, 1097 (1969).
[20] W. H. E. Schwarz and R. J. Buenker, Chem. Phys. **13**, 153 (1976).
[21] I. V. Schweigert and S. Mukamel, Phys. Rev. A **77**, 033802 (2008).
[22] G. D. Mahan, *Many Particle Physics* (Plenum, New York, 1983).
[23] W. H. E. Schwarz, L. Mensching, K. H. Hallmeier, and R. Szargan, Chem. Phys. **82**, 57 (1983).
[24] I. V. Schweigert and S. Mukamel, Phys. Rev. A **76**, 012504 (2007).
[25] B. Brena, Y. Luo, M. Nyberg, S. Carniato, K. Nilson, Y. Alfredsson, J. Ahlund, N. Martensson, H. Siegbahn, and C. Puglia, Phys. Rev. B **70**, 195214 (2004).
[26] L. Campbell and S. Mukamel, J. Chem. Phys. **121**, 12323 (2004).
[27] R. K. Pandey and S. Mukamel, J. Chem. Phys. **124**, 094106 (2006).
[28] I. V. Schweigert and S. Mukamel (unpublished).
[29] N. T. Maitra, F. Zhang, R. J. Cave, and K. Burke, J. Chem. Phys. **120**, 5932 (2004).
[30] A. D. Becke, J. Chem. Phys. **98**, 5648 (1993).
[31] W. J. Hehre, R. Ditchfield, and J. A. Pople, J. Chem. Phys. **56**, 2257 (1972).
[32] M. J. Frisch, G. W. Trucks, H. B. Schlegel *et al.*, GAUSSIAN 03, Revision C.02, Gaussian, Inc., Wallingford, CT, 2004.
[33] J. T. Francis and A. P. Hitchcock, J. Phys. Chem. **96**, 6598 (1992).
[34] C. C. Turci, S. G. Urquhart, and A. P. Hitchcock, Can. J. Chem. **74**, 851 (1996).
[35] See EPAPS Document No. E-JCPSA6-128-506808 for the real, imaginary and absolute value N/O signals of para-aminophenol. This document can be reached through a direct link in the online article's HTML reference section or via the EPAPS homepage (http://www.aip.org/pubservs/epaps.html).